Some Ion-Beam Modification Issues: Ion-Induced Amorphisation and Crystallisation of Silicon

J.S. Williams*, G. de M. Azevedo[1] and A. Kinomura[2]

Research School of Physical Sciences and Engineering
Australian National University, Canberra, 0200 Australia
[1]Present address: Brazilian Synchrotron Light Laboratory (LNLS), 6192–CEP 13084-971, Campinas, SP, Brazil
[2]Present address: Advanced Defect-Characterization Research Group
Research Institute of Instrumentation Frontier
National Institute of Advanced Industrial Science and Technology
1-1-1 Umezono, Tsukuba, Ibaraki 305-8568, Japan

Abstract

This paper reviews the crystalline to amorphous and amorphous to crystalline phase transformations which can be induced in silicon by energetic ion irradiation. An overview of ion disordering and amorphisation is treated first. At temperatures or irradiation conditions under which the defects generated by the ion bombardment are relatively stable, disorder builds up with ion dose until complete amorphisation occurs. At elevated temperatures, the disordering and amorphisation processes can be considerably more complex. In this regime, dynamic annealing can occur during irradiation, whereby defects can annihilate and cluster to form defect bands. If the temperature is not too high, amorphisation can be nucleated with increasing dose at such defect bands but also at surfaces and interfaces, often well away from the maximum in the (nuclear) energy deposition distribution. Such nucleation-limited amorphisation is difficult to model, particularly as the critical dose for amorphisation depends in a complex way on irradiation temperature, ion mass, ion energy and ion flux. Once an amorphous layer forms

* E-mail: director.RSPSE@anu.edu.au

in this regime, it can extend with increasing dose in a layer-by-layer manner. Again, there is no accepted model for this process. At higher irradiation temperatures, crystallisation of pre-existing amorphous layers can be induced. This ion beam induced epitaxial crystallisation (IBIEC) process occurs at temperatures well below that at which normal thermal epitaxial crystallisation takes place. This paper then gives an overview of the experiments and observations that have been made to study the IBIEC phenomenon. Studies of the dependence of the growth rate on irradiation temperature, ion dose, ion mass and ion flux again point to a complex process, but it is clear that the crystallisation is induced by ion displacements at or close to the amorphous-crystalline interface. Irradiations under ion channeling conditions, coupled with simulations of displacement distributions, have been used to probe the mechanism in more detail. Although it is now possible to establish that ion-induced defect generation precisely at the amorphous-crystalline interface is responsible for IBIEC, modelling of the process is again difficult. Such difficulties result from complex temperature, ion mass and flux dependencies, whereby the density of the collision cascade and inter-cascade effects appear to play dominant roles. Although much is known about both ion-induced amorphisation and crystallisation processes, the observed dependencies over a broad temperature range cannot as yet be quantitatively modelled.

Contents

1 Introduction **229**

2 Overview of Ion-Induced Amorphisation **230**
2.1 The Effect of Temperature on Defect Accumulation 230
2.2 Preferential Amorphisation at Surfaces and Defect Bands 232
2.3 Mechanisms of Amorphisation: The Role of Defects 234
2.4 Layer-by-Layer Amorphisation 237

3 Overview of Ion Beam Induced Epitaxial Crystallisation **239**
3.1 IBIEC Temperature Dependence 239
3.2 IBIEC Observations and Dependencies 239
3.3 IBIEC and Early Channeling Studies 245
3.4 IBIEC Models 248

4 Cascade Effects on IBIEC: Observations and Interpretation **249**
4.1 Experimental Observations 249
4.2 Comparison with Simulations 252

5 Some Answered and Unanswered Questions **257**

References **258**

1. Introduction

When materials are irradiated with energetic ions, the ion-induced disorder can lead to a number of interesting structural transformations, including amorphisation and crystallisation. The behaviour is particularly interesting when irradiation is carried out at temperatures where the defects produced by the ion beam are mobile. Silicon is an ideal material to observe and understand such processes, but, despite extensive studies over the past two decades, there are still many unanswered questions relating to ion-induced defects and their influence on amorphisation and crystallisation. For ion irradiation at or below room temperature in silicon, the disorder produced is essentially stable since point defects are readily immobilised within disordered regions. Under such conditions, ion damage generated within collision cascades builds up with ion dose, leading to amorphisation of the silicon. At higher implant temperatures, where defects begin to move and interact during ion bombardment, significant defect annihilation can occur and it can be difficult to induce amorphisation. In this regime, preferential amorphisation can be observed at regions where extended defects first form, for example, at nanocavities or at surfaces. Continued irradiation can lead to layer-by-layer amorphisation.

At even higher temperatures ion irradiation may not cause amorphisation. Incomplete defect annihilation during bombardment can lead to the formation of defect clusters and even extended defects in an otherwise crystalline matrix. In this elevated temperature regime, where defects are mobile, the understanding of the observed defect-mediated processes is far from complete. Irradiation under these conditions can even lead to the recrystallisation of previously-amorphised layers. This latter process, so called ion-beam-induced-epitaxial crystallisation (IBIEC), occurs at temperatures well below that at which normal thermally-induced crystallisation of amorphous silicon occurs. IBIEC has been shown to be an activated process, dependent on the generation of mobile "defects" by ion irradiation. There has been considerable controversy as to the role of defects in IBIEC but recent experiments have assisted in partly clarifying this issue. Indeed, studies of ion-induced amorphisation and crystallisation not only indicate much about the behaviour of defects and defect-induced phase changes in silicon but also provide considerable insight into the fundamental physics of defect interactions and epitaxial crystallisation at an atomic level. This review first gives an

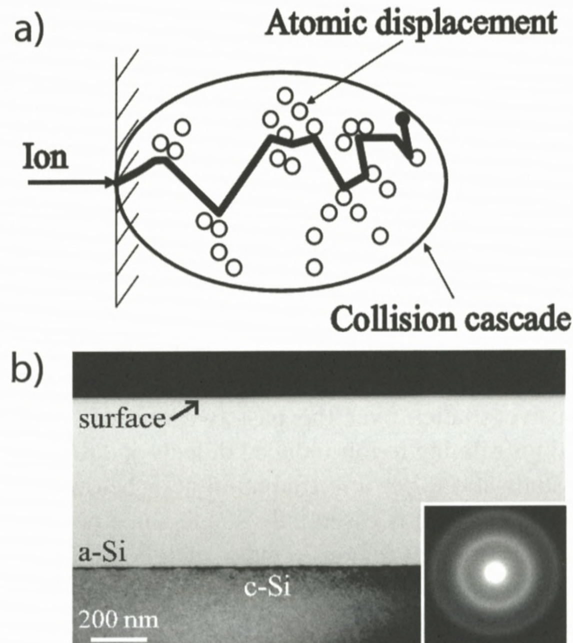

Figure 1. (a) Schematic of displacements within a collision cascade. (b) A cross-sectional transmission electron microscope (XTEM) image of a continuous amorphous layer (a-Si) generated in silicon by 245 keV Si ion irradiation at room temperature to a dose of 3×10^{15} cm^{-2}. The sample surface is indicated, as is the underlying crystalline silicon (c-Si).

overview of ion-induced amorphisation and crystallisation phenomena that have been observed in silicon and identifies some unanswered questions. More recent experiments, that provide insight into both ion-induced defect interactions and IBIEC, are then presented and interpreted with the aid of computer simulations. Finally, a summation of what is known and what is not known in these areas is presented.

2. Overview of Ion-Induced Amorphisation

2.1. The Effect of Temperature on Defect Accumulation

At sufficiently low irradiation temperatures, residual lattice disorder in semiconductors is controlled by the energy deposited by swift ions in nuclear collisions with lattice atoms. Individual heavy ions can generate dense displacement cascades (Figure 1a) that result directly in amorphous zones (Howe and Rainville,

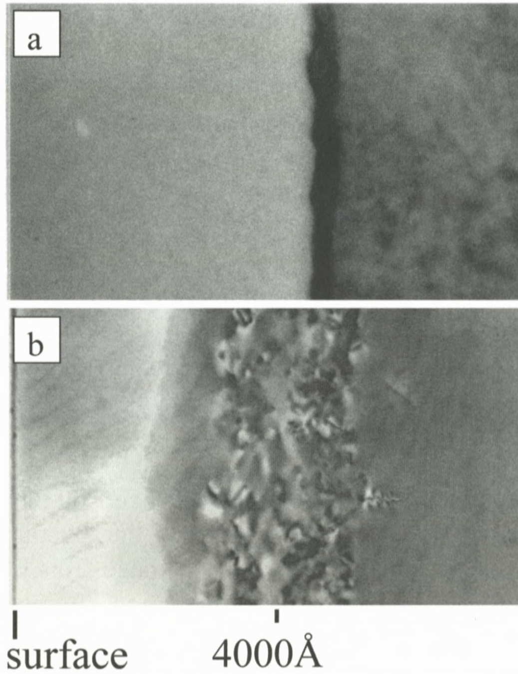

Figure 2. XTEM images corresponding to 245 keV Si ion irradiation of silicon (100) to a dose of $4 \times 10^{15}\text{cm}^{-2}$ at (a) room temperature, and (b) 350°C. After Williams (1998).

1987) and the overlap of such zones with increasing dose leads to a continuous amorphous layer (Morehead et al., 1970; Dennis and Hale, 1978), as shown in the cross-sectional transmission electron micrograph (XTEM) in Figure 1b. For light ions, cascades are less dense and the lattice can collapse to an amorphous phase when a sufficiently high defect density builds up and the local free energy of the defective lattice exceeds that of the amorphous phase (Swanson and Quennevi, 1971; Vook and Stein, 1969; Christel et al., 1981). These two extremes of damage build up at low temperatures can be successfully treated by heterogeneous (heavy ion) or homogeneous (light ion) models, such as those of Morehead et al. (1970) and Vook and Stein (1969), respectively.

Implantation temperature can determine whether the defects generated within collision cascades are stable or whether they can migrate and annihilate. An example of temperature dependent effects is shown in Figure 2 (Williams, 1998). Figure 2a is a XTEM micrograph depicting a continuous amorphous layer in silicon, produced by 245 keV Si ions at room temperature to a dose of $4 \times 10^{15}\ \text{cm}^{-2}$. The ion range is around 3800 Å but, under these implant conditions,

the amorphous layer is around 5000 Å thick. Note that the boundary between the amorphous layer and the underlying silicon substrate is quite sharp, indicating that defects produced in the tail of the Si implant distribution can annihilate quite effectively at this implant temperature. If the implant temperature is raised to 350°C, irradiation-produced defects are considerably more mobile and annihilate or cluster to effectively suppress amorphisation (Williams 1992), as shown in the XTEM micrograph in Figure 2b. Here, there are clearly observed interstitial clusters that evolve into well defined interstitial-based line defects such as {311} defects and dislocation loops (Takeda et al., 1994) on annealing. It will be shown later that, at such implant temperatures where defects can annihilate, irradiation-induced displacements can induce crystallisation of pre-existing amorphous layers.

Between the two extreme regimes illustrated in Figure 2, the close balance between the rate of damage production within collision cascades and the rate of dynamic annealing (defect annihilation and clustering) can give rise to interesting defect-mediated phenomena, with strong dependencies on implantation temperature, dose and dose rate. Small changes in any of these parameters can result in dramatic differences in residual implantation damage from almost damage-free structures, as a result of efficient defect annihilation, to continuous amorphous layers. In this regime, amorphisation can occur in an entirely different way, as a result of nucleation-limited or preferential amorphisation processes (Goldberg et al., 1999). For example, as the implantation dose increases and the density of defects increases, amorphous layers can spontaneously form at the depth of maximum disorder. Such layers can then grow to encompass the entire defective region (Goldberg et al., 1995). Further examples of the critical balance between defect creation and defect annihilation, including preferential amorphisation, are given below.

2.2. Preferential Amorphisation at Surfaces and Defect Bands

Amorphous layers can be observed to nucleate preferentially at depths significantly away from the maximum in the ion's energy deposition distribution, at, for example, surfaces (Williams et al., 1994b), interfaces and pre-existing defects (Goldberg et al., 1999; Williams et al., 1994a). Figure 3 illustrates the case of preferential amorphisation at a silicon surface or, more precisely, at a SiO_2-Si interface. Figure 3a (Goldberg et al., 1995) shows an RBS/channeling spectrum for an 80 keV Si implant into silicon at 160°C for a dose of 10^{16} cm^{-2} at a beam flux of 2.7×10^{13} ions cm^{-2} s^{-1}. The spectrum shows a strong disorder peak at the surface and a buried peak around the end-of-ion-range at about 1200 Å. (The end-of-ion-range refers to the region in the tail of the ion range distribution, about two standard deviations deeper than the projected ion range.) The corresponding

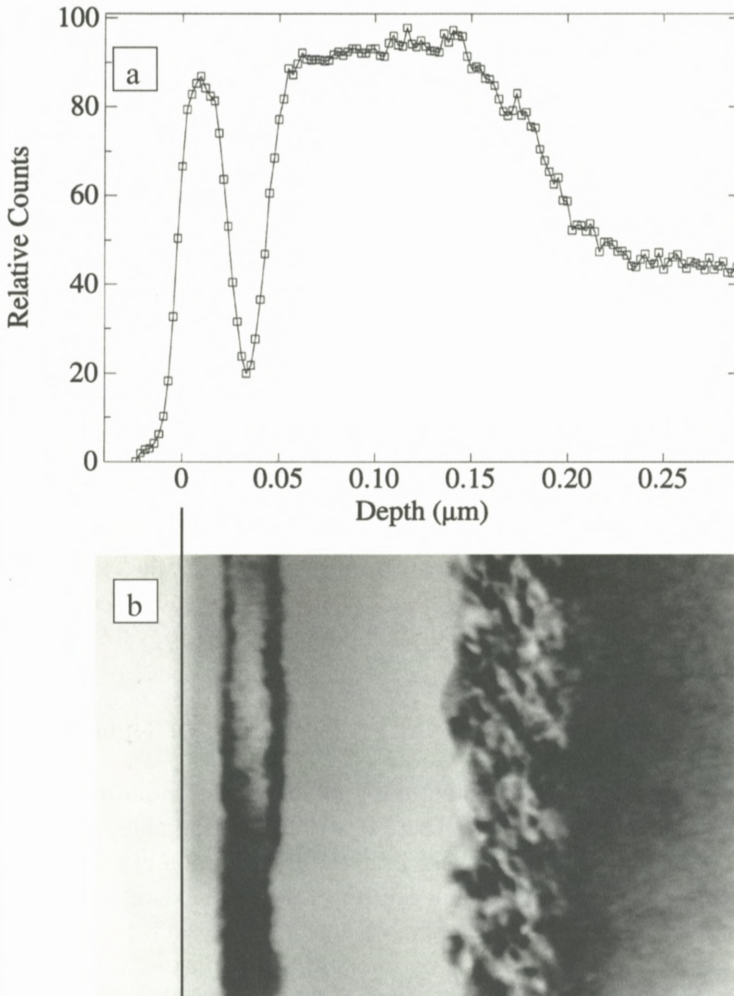

Figure 3. (a) An RBS/channeling spectrum for an 80 keV Si implant into silicon at 160°C to a dose of 10^{16} cm^{-2} at a beam flux of 2.7×10^{13} ions cm^{-2} s^{-1}. After Goldberg et al. (1995). (b) XTEM image of the sample in (a). After Goldberg (1995).

XTEM micrograph in Figure 3b (Goldberg, 1995) indicates that there are two amorphous layers present, one extending 300 Å from the surface and a buried layer from 500 to 1500 Å. Between these layers is a region of crystalline silicon containing few defects but below the buried layer there is a region of crystalline silicon, rich in (interstitial-type) defect clusters. This result shows not only the

nucleation of an amorphous region around the maximum in the nuclear energy distribution at about 800 Å but nucleation of an amorphous layer well away from the maximum disorder depth, at the surface. When the evolution of this defect structure was examined as a function of ion dose (Goldberg, 1995), it was found that the deep disorder first accumulated as defect clusters of interstitial character at lower doses. This defective region then appeared to collapse into an amorphous layer as the dose increased. In addition, the surface amorphous layer was found to thicken with increasing dose. This behaviour suggests that, in a regime where substantial dynamic annealing occurs during ion irradiation, mobile defects not only annihilate and locally form defect clusters, but can also migrate and accumulate at SiO_2-Si interfaces. Collapse of such disorder to an amorphous phase can occur at a sufficiently high implantation dose. It has also been shown that a pre-existing dislocation band can act as a nucleation site for amorphisation, even when it is situated well away from the disorder peak (Goldberg et al., 1999). Furthermore, such dislocation bands were found to “getter” interstitial-based defects from deeper in the material during irradiation (Goldberg et al., 1999). Thus, it would appear that both dislocation bands, surfaces (actually SiO_2-Si interfaces) and amorphous layers themselves are good trapping sites or sinks for mobile defects that may otherwise form stable clusters close to where they come to rest, in the absence of such sinks.

2.3. Mechanisms of Amorphisation: The Role of Defects

The mechanism for the above defect trapping and preferential amorphisation behaviour deserves some comment. There has been considerable speculation in the literature (Williams, 1992; Goldberg et al., 1999; Elliman et al., 1988; Jackson, 1988) as to the specific defects that are trapped at pre-existing defects, surfaces and amorphous layers. Clearly, open volume defects such as vacancies or divacancies, as well as interstitials or interstitial complexes, are candidates. As we discuss more fully below, some experiments on the kinetics of amorphous layer formation, in the regime where the irradiation-induced amorphous phase is nucleation-limited, have suggested that divacancies (Elliman et al., 1988) may be the main defects preferentially trapped at amorphous layers. However, other experiments, where amorphous layers are nucleated at pre-existing dislocation bands, suggest (Goldberg et al., 1999) that interstitial trapping also may have a major role to play. Nevertheless, regardless of the specific defects that accumulate prior to amorphisation, it would appear to be the local free energy that ultimately determines the collapse of a defective crystalline lattice to the amorphous phase. This mechanism (Williams, 1994) is illustrated schematically in Figure 4. The free energy of an amorphous phase exceeds that of a crystalline phase. In the

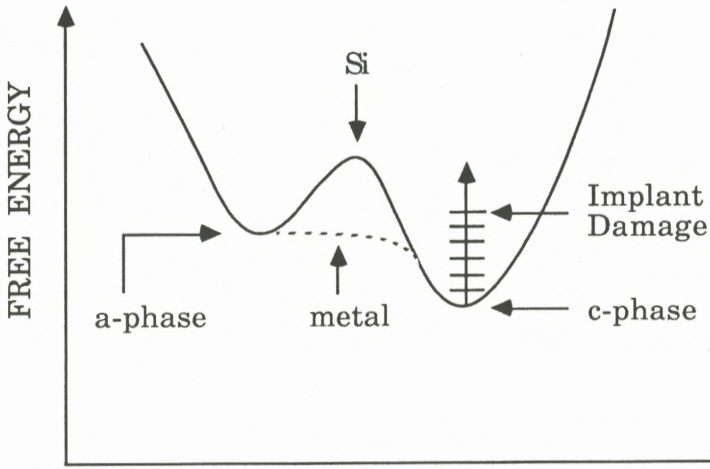

Figure 4. Schematic illustrating free energy differences and pathways between amorphous and crystalline materials. After Williams (1994).

case of silicon, the amorphous phase is metastable since there is a kinetic barrier that must be overcome before crystallisation can occur. In contrast, for pure metals, an amorphous phase is unstable even at extremely low temperatures, since there is essentially no barrier to crystallisation. Thus, under appropriate implantation conditions, implantation-induced disorder in silicon can build up until the local free energy exceeds that of the amorphous phase. It can then be energetically favourable for the defective crystalline lattice to collapse to the amorphous phase that provides a local minimum in free energy. Such behaviour suggests that, in cases where there is some defect mobility, defect annihilation and agglomeration occurs and the amorphous phase can preferentially form at sites which minimise the local free energy. Under such situations amorphisation can be nucleation-limited.

In cases where there are no pre-existing nucleation sites for amorphisation, the onset of amorphisation (at elevated temperatures) usually occurs at the ion-end-of-range. Here, nucleation of the amorphous phase normally occurs where there is an interstitial excess and this corresponds roughly to the end-of-ion-range. In this regime, amorphisation can exhibit interesting dependencies, including situations where the ion flux controls the critical amorphisation temperature (Elliman et al., 1988), as illustrated in Figure 5. For a fixed dose of 5×10^{15} cm^{-2} for 1.5 MeV Xe ions irradiating silicon, amorphisation at the end-of-ion-range can be observed only below 200°C if the average beam flux is kept below 10^{12} ions

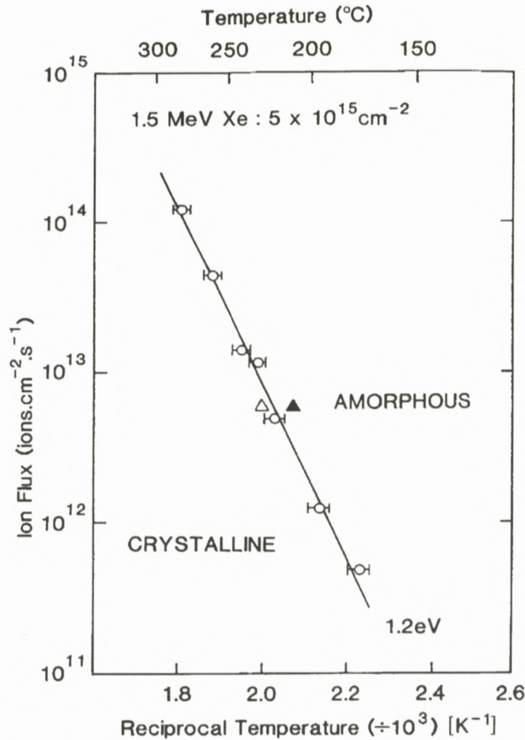

Figure 5. Ion flux as a function of $1/T$ for ion irradiation conditions (1.5 MeV Xe ions at a dose of 5×10^{15} cm^{-2}) under which a buried amorphous layer is just formed in silicon. The solid and open triangles represent the cases in Figures 7b and 8b, respectively. After Elliman et al. (1988).

cm^{-2} s^{-1}, but up to 300°C if the ion flux is raised above 10^{14} ions cm^{-2} s^{-1}. This demonstrates the critical dependence of amorphisation on the balance between the rate of disorder production (controlled by ion flux in the case of Figure 5) and the extent of dynamic annealing, which is controlled by irradiation temperature. For implantation conditions on the left hand side of the solid line in Figure 5, no amorphous silicon was formed (only defect clusters in crystalline silicon), whereas buried amorphous layers are generated under conditions on the right. Note that the onset of amorphisation in Figure 5 fits well to an activation energy of 1.2 eV. Elliman et al. (1988) noted that this value corresponds to the dissociation energy of silicon divacancies and, consequently, suggested that the stability of divacancies may control amorphisation in silicon. However, more recent studies, that use other ion beams to examine the dependence of the onset of amorphisation on ion flux and temperature, have shown a range of activation energies between

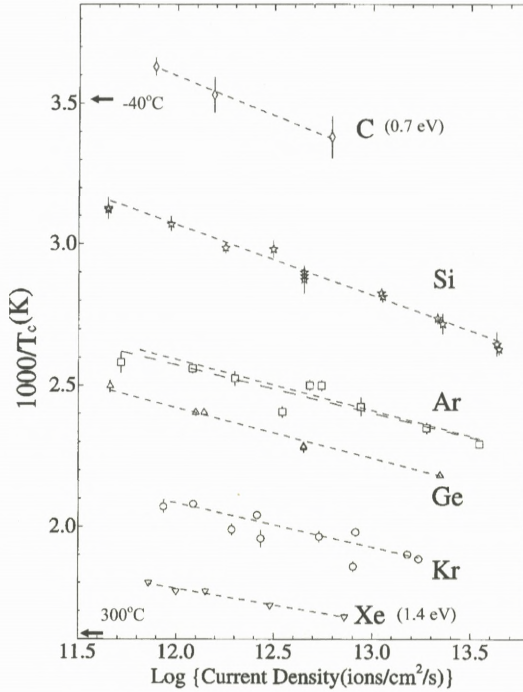

Figure 6. Ion flux as a function of $1/T$ for ion irradiation conditions under which a buried amorphous layer is just formed in silicon for a number of ions at a dose of 10^{15} cm^{-2} except C where the dose was 2×10^{15} cm^{-2}. After Goldberg et al. (1993).

0.5 and 1.7 eV as shown in Figure 6, taken from the work of Goldberg et al. (1993). The conclusion is that more complex defects and defect interaction processes may control amorphisation, depending on the implant conditions used, particularly the implantation temperature.

2.4. Layer-by-Layer Amorphisation

Another intriguing case of preferential amorphisation is layer-by-layer amorphisation, which has been observed in some cases when silicon containing pre-existing amorphous layers is re-irradiated at elevated temperatures (Linnros et al., 1988b). An example of such behaviour is illustrated by the XTEM micrographs in Figure 7 (Elliman et al., 1987). Clearly, the near-surface amorphous layer in Figure 7a has increased in thickness when irradiated with 1.5 MeV Xe ions at 208°C (Figure 7b). It is also interesting to note that a buried amorphous layer has also formed at the Xe end-of-ion-range under these conditions. The region between

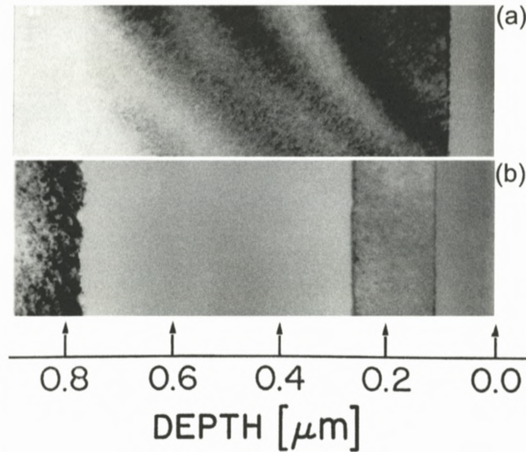

Figure 7. XTEM images illustrating layer-by-layer amorphisation of silicon by 1.5 MeV Xe ion irradiation to a dose of 5×10^{15} cm^{-2}. (a) A pre-existing surface amorphous layer on silicon prior to Xe irradiation, and (b) following Xe irradiation at 208oC. After Elliman et al. (1987).

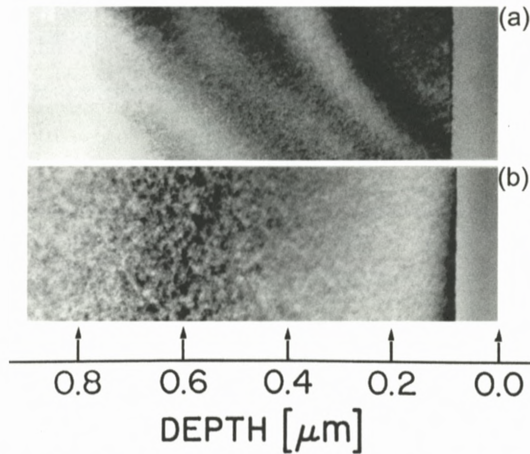

Figure 8. XTEM images illustrating IBIEC of a pre-existing amorphous layer in silicon (a) using 1.5 MeV Xe ions to a dose of 5×10^{15} cm^{-2} at a temperature of 227°C. After Elliman et al. (1987).

the two amorphous layers is essentially free of defects, as a result of near perfect defect annihilation in this region. Both amorphous layers are observed to extend layer-by-layer with increasing ion dose, presumably by the preferential trapping of mobile defects at the respective amorphous-crystalline interfaces.

3. Overview of Ion Beam Induced Epitaxial Crystallisation

3.1. IBIEC Temperature Dependence

The previous section illustrated implantation conditions where amorphisation by ion irradiation is nucleation-limited and can give rise to preferential amorphisation and layer-by-layer amorphisation phenomena. If the implantation conditions are changed to further favour the rate of dynamic annealing over defect production, by raising the temperature for example, pre-existing amorphous layers can be observed to crystallise epitaxially by the IBIEC process. IBIEC is illustrated for the case of 1.5 MeV Xe irradiation in Figure 8 (Elliman et al., 1987). At an irradiation temperature of 227°C, the pre-existing surface amorphous layer is observed to shrink. Increasing the dose causes further epitaxial growth of the amorphous layer. It is interesting to note that a slight reduction in irradiation temperature to 208°C, keeping the other irradiation conditions the same, induces layer-by-layer amorphisation, as previously shown in Figure 7. If the temperature is increased further, above that corresponding to the data in Figure 7b, the IBIEC rate speeds up. The temperature dependence of IBIEC is illustrated in Figure 9 for the case of 600 keV Ne irradiation of silicon (Williams et al., 1985b). Note that a well-defined activation energy can be extracted from the data (0.24 eV), the magnitude of which is suggestive that defect-mediated processes control IBIEC, possibly vacancies (Elliman et al., 1987; Williams et al., 1985b). In Figure 9, the kinetics of thermally-induced epitaxial growth is also shown, with the normal activation energy of 2.8 eV (Olson and Roth, 1988). It was accepted in early IBIEC studies (Williams et al., 1985b; Olson and Roth, 1988) that the low IBIEC activation energy arose as a result of athermally generated displacements. These displacements provide the defects for stimulating bonding rearrangements at the interface and hence crystallisation. In the thermal case, the high activation energy was attributed (Williams et al., 1985b) to two activation terms, nucleation of the defects influencing epitaxial crystallisation and a second term involving migration and bond rearrangement. In IBIEC, the first term is eliminated by athermal defect generation and only the second activation term applies. More detailed treatment of IBIEC mechanisms will be given in Section 3.4.

3.2. IBIEC Observations and Dependencies

Early studies (Linnros et al., 1985, 1988b; Elliman et al., 1987; Williams et al., 1985b; Priolo et al., 1989b) indicated that the IBIEC rate was proportional to ion dose and was controlled by nuclear energy deposition. This demonstrates that atomic displacements are crucial for IBIEC. Indeed, experiments with electron

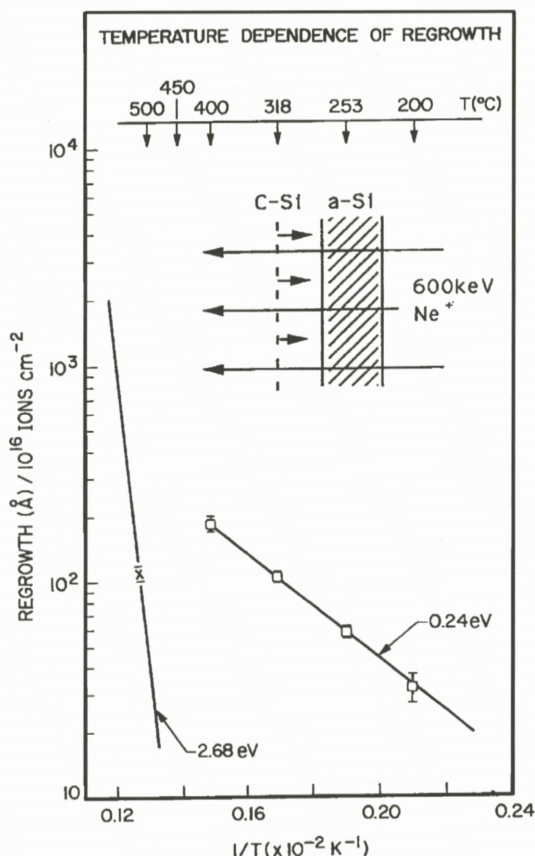

Figure 9. IBIEC regrowth for a dose of 10^{16} Ne ions cm^{-2} (600 keV) as a function of $1/T$ (open squares) in silicon. The activation energy for thermally-induced epitaxy (2.8 eV) is also shown. After Williams et al. (1985b).

beams (Lulli et al., 1987) have clearly shown that recrystallisation only occurs if the energy of the electron beam is sufficient to produce atomic displacements in silicon in the region of the amorphous-crystalline interface. Several studies (Linnros et al., 1985, 1988b; Elliman et al., 1987; Williams et al., 1985b; Priolo et al., 1989b; Lulli et al., 1987; Priolo and Rimini, 1990) have suggested that atomic displacements generated by nuclear collisions very close to the amorphous-crystalline interface are responsible for IBIEC. For example, Figure 10 from Williams et al. (1985a) shows the dependence of IBIEC on nuclear energy deposition at the interface. In Figure 10a, the RBS/channeling spectra show that for 1.5 MeV Ne ions at 318oC the extent of regrowth is linear with dose for this

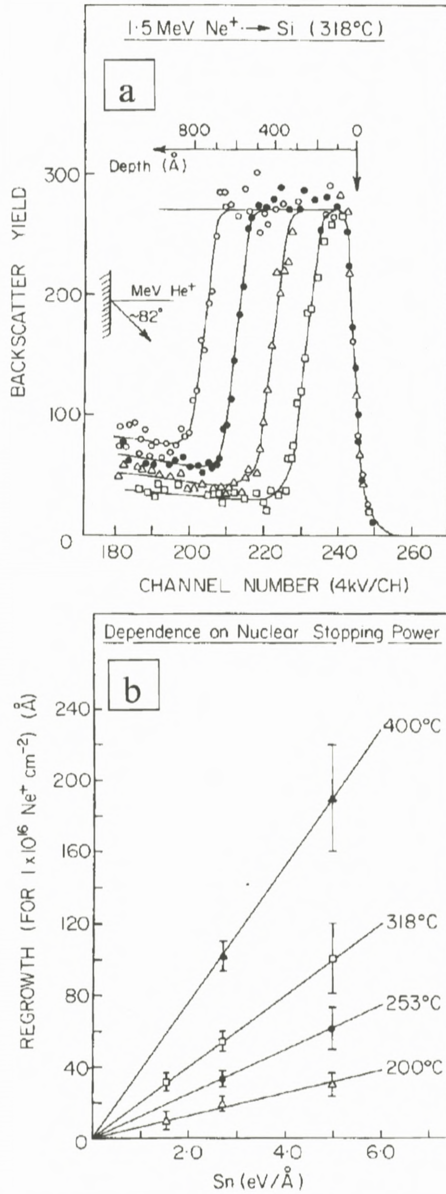

Figure 10. (a) RBS/channeling spectra from a silicon sample (with a pre-amorphised layer) held at 318°C and irradiated sequentially with 1.5 MeV Ne ions at dose increments of 3×10^{16} cm^{-2}. The open circles data show the spectrum corresponding to the pre-existing amorphous layer. (b) IBIEC growth normalised to a Ne dose of 10^{16} cm^{-2} as a function of nuclear stopping power (S_n) for different substrate temperatures. After Williams et al. (1985a).

irradiation situation, where the nuclear energy deposition is relatively constant at the interface as regrowth proceeds. In Figure 10b, IBIEC growth is plotted as a function of nuclear energy deposition at the interface (Sn) for Ne ion irradiation at 4 temperatures. Here, three Ne ion energies were used (0.6, 1.5 and 3 MeV) and the atomic displacements generated by the ion beam at the amorphous-crystalline interface (Sn) were obtained from simulations using the TRIM code (Ziegler et al., 1985). The IBIEC rate is observed to scale with the nuclear energy deposition at the interface. This result strongly suggests that long range diffusion of defects from the amorphous or crystalline sides of the interface do not contribute significantly to IBIEC but does not rule out short range diffusion, an issue we return to later.

The IBIEC growth rate is also found to be significantly different for different substrate orientations (Priolo et al., 1989b; Cannavo et al., 1986; Maher et al., 1987), where a 2–4 times slower rate is observed for ⟨111⟩ compared with ⟨100⟩ orientations. No difference between ⟨100⟩ and ⟨110⟩ orientations is observed for IBIEC. These trends are somewhat similar to those found in normal thermally-induced epitaxial growth but the scale of the difference is greater for thermal epitaxy, where a 25 times difference in rates between ⟨111⟩ and ⟨100⟩ substrates is obtained and there is also a 2.5 times difference between ⟨110⟩ and ⟨100⟩ substrates (Olson and Roth, 1988). Furthermore, the slower rates of thermally-induced epitaxial growth observed in ⟨111⟩ oriented layers are consistent with models which suggest that solid phase epitaxy is mediated by bond breaking and remaking processes at kinks and ledges on the amorphous-crystalline interface (Spaepen and Turnbull, 1982; Williams and Elliman, 1983). Indeed, the interface is expected to be resolved into surfaces of minimum free-energy by the formation of terraces with a {111} orientation and epitaxial growth proceeds by thermally activated atomic rearrangements at energetically favourable kink sites on ledges connecting two consecutive (111) terraces, as proposed in the phenomenological models of Spaepen and Turnbull (1982) and Williams and Elliman (1983). Rate differences arise from the different concentrations of kink sites, depending on the interface geometry or orientation. Priolo et al. (1990) have suggested that similar processes may account for the IBIEC orientation dependence.

The effects of impurity species on IBIEC are also qualitatively similar to those observed for thermal epitaxy (Olson and Roth, 1988; Kennedy et al., 1977; Poate et al., 1987). For example, slow diffusing electrically active dopants, such as B and P, are observed to enhance the IBIEC growth rate (Priolo et al., 1990), whereas species such as oxygen, that form strong bonds with silicon, are observed to retard the rate (Priolo et al., 1989a). However, the magnitudes of the rate changes are considerably smaller than those observed for thermal epitaxy, again suggesting

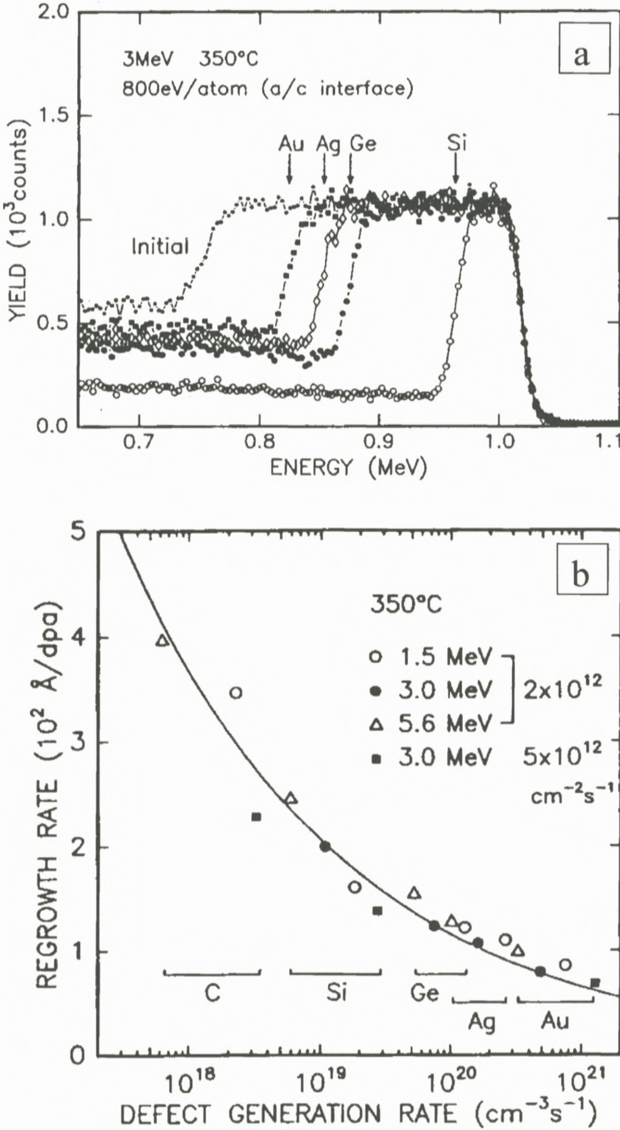

Figure 11. (a) Channeling spectra showing the difference in regrowth thicknesses among four different ion species (Au, Ag, Ge, and Si) at 3.0 MeV. Irradiation doses were adjusted to provide the same total nuclear energy deposition (800 eV per atom) to the initial amorphous/crystalline interfaces. (b) Normalised regrowth rates as a function of defect generation rate for five ion species (C, Si, Ge, Ag, and Au) at three energies (1.5, 3.0, and 5.6 MeV) with two dose rates (2×10^{12} and 5×10^{12} cm^{-2} s^{-1}). After Kinomura et al. (1999).

that the lower temperatures of IBIEC growth may not achieve thermal equilibrium behaviour (Priolo and Rimini, 1990). Priolo and Rimini (1990) have also reviewed the IBIEC behaviour of fast diffusing species, such as Au and Ag, and again noted the similar tendency for such impurities to strongly prefer to remain in the amorphous phase as growth proceeds. This leads to segregation at the moving amorphous-crystalline interface. IBIEC allows such segregation phenomena to be studied at low temperatures, where the interface velocity can exceed the impurity diffusivity in the amorphous phase (Poate et al., 1988). These intriguing impurity segregation effects are not further treated in this paper, which concentrates more on the mechanisms of IBIEC.

Although studies of the energy and depth dependence of IBIEC growth, such as that in Figure 10, indicate that the IBIEC rate scales with nuclear energy deposition, such scaling across widely different ion masses does not occur. Indeed, ion mass effects were appreciated early (Linnros et al., 1988a), but only relatively recently have they been quantified in terms of an influence of cascade density on IBIEC rate (Kinomura et al., 1999). Furthermore, a small ion flux dependence of IBIEC (Linnros et al., 1988a, 1988b) was also found in early studies and the scale of this effect has only recently been examined over a wide flux range (Kinomura et al., 1999; Heera et al., 1993). Such mass effects, which illustrate the role of cascade density on IBIEC, and flux effects, which indicate the interaction times of defects contributing to IBIEC, are illustrated in Figure 11, taken from the work of Kinomura et al. (1999). Figure 11a shows RBS/channeling spectra that illustrate the mass dependence of IBIEC. Here 3 MeV Au, Ag, Ge and Si ions were used to irradiate an amorphous silicon layer of about 2000 Å in thickness on a silicon ⟨100⟩ substrate. Different doses were chosen to provide the same total nuclear energy deposition at the amorphous-crystalline interface and MeV ions were chosen to provide a near constant energy deposition at the interface during IBIEC growth. It is clear from Figure 11a that the regrown thickness increases with decreasing ion mass, even though the total nuclear energy deposition is similar for each ion within the range of the measured depth. This clearly shows that, at the same average ion flux, the *rate* of nuclear energy deposition, or the cascade density, clearly influences IBIEC. Another effect observed by Kinomura et al. (1999) was a flux dependence, whereby higher fluxes of the same ions under otherwise identical conditions resulted in less regrowth. This is again consistent with the observation that the rate of nuclear energy deposition influences IBIEC. Figure 11b plots the IBIEC regrowth rate (normalised to constant nuclear energy deposition at the interface) as a function of defect (ie vacancy) generation rate at the interface for five ion masses, four ion energies and two fluxes at 350°C. The defect generation was calculated using TRIM (Ziegler et al., 1985). Note that

the defect generation rate varies over more than 4 orders of magnitude from C to Au and the normalised growth rate for C is about 4 times that of Au under these conditions. A similar dose rate dependence for 300 keV ions has also been demonstrated by Linnros and Hólmen (1986) and Heera et al. (1993). Furthermore, Heera et al. (1995) proposed a diffusion limited model to explain IBIEC, where the regrowth thickness, normalised to dose, was proportional to ion beam current to the $-1/4$ power. Kinomura et al. (1999) have extended this treatment and the solid curve in Figure 11b is a fit to the equation

$$r_{\mathrm{d}} = cg^{-1/4}, \tag{1}$$

where r_{d} is the regrowth thickness normalised to the number of displacements, c is a constant and g is the defect generation rate. The curve is a good fit to the data points for the conditions employed in Figure 11b but, as we show below, it does not fit particularly well to more extended dose rate data.

As indicated in Figure 11b, there are two parameters that conveniently change the defect generation rate, namely ion mass and ion flux. Figure 11b would appear to indicate that these different ways of changing defect generation rate, by altering cascade density (instantaneous displacement density within a single collision cascade) and ion flux (which changes the average time between the spatial overlap of subsequent cascades), have similar effects on IBIEC. However, Kinimora et al. (1999) subsequently varied the ion flux for similar mass ions over a wide range and found that cascade density and ion flux changes do not give identical changes to IBIEC rates. These results are shown in Figure 12a for Au and Ag ions, where the IBIEC rate seems to vary linearly with defect generation rate rather than the proposed Heera et al. (1995) fit. These data suggest that cascade size and ion flux give rise to separate influences on IBIEC rate, in addition to their common influence on defect generation rate, as we discuss more fully below. In Figure 12b we illustrate another case where more extensive recent data provide further insight into IBIEC processes. These data show that the apparent activation energy of IBIEC extracted from temperature dependent studies can vary from 0.18 to 0.4 eV, depending on ion mass. We also discuss the significance of these observations in the discussion of IBIEC mechanisms in Section 3.4.

3.3. IBIEC and Early Channeling Studies

A further series of observations relate to the influence of channeling of the incident ion beam on IBIEC rate. Experiments under channeling conditions can, in principle, help to clarify where the defects that influence IBIEC are generated, since channeling allows selective reduction in the number of defects produced in the crystalline region. However, in the early measurements using channeling

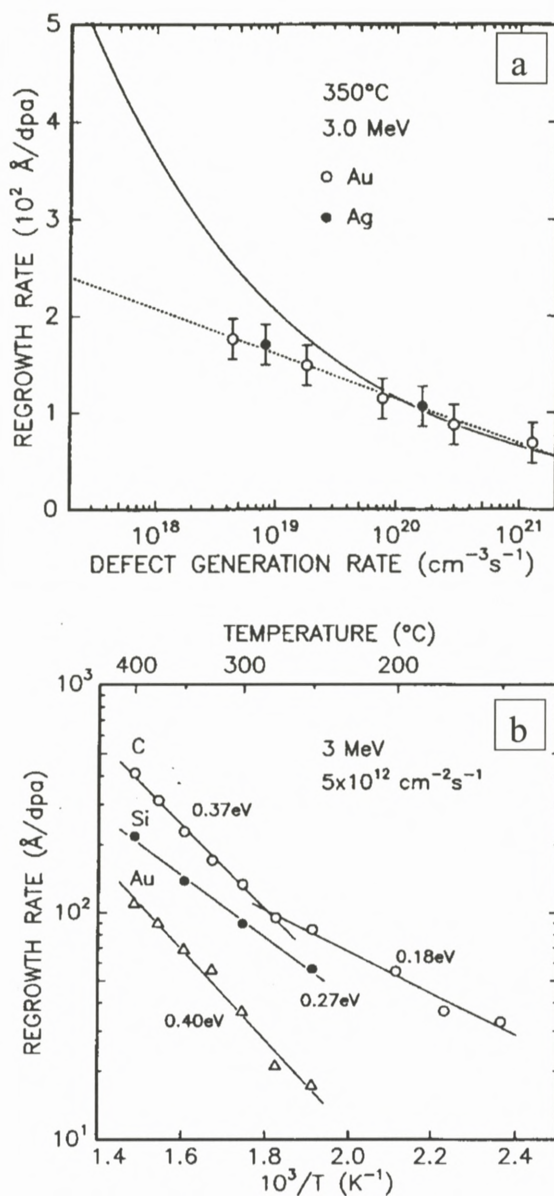

Figure 12. (a) Dose rate dependence of IBIEC for 3.0 MeV Au and Ag compared with the fitting curve of Figure 11b (solid curve). (b) Temperature dependence of IBIEC regrowth rates normalised to the number of displacements for 3.0 MeV Si, Ge and Au with a dose rate of 2×10^{12} cm^{-2} s^{-1}. After Kinomura et al. (1999).

(Williams et al., 1985b; Linnros and Hólmen, 1986; Elliman et al., 1986), the interpretation of the results has not been conclusive, mainly because it was difficult to estimate the exact number of point defects generated in the crystalline region, particularly after an ion beam had traversed an amorphous layer before entering the crystal. In cases of a surface amorphous layer and the incident beam aligned with a channeling direction in the underlying crystal, the IBIEC rate appeared to be reduced in some cases (Linnros and Hólmen, 1986) and not in others (Williams et al., 1985b). The multiple scattering of the beam in the amorphous layers was suggested as a reason for such differences and hence defects migrating short distances to the interface from the crystalline side of the interface may still play a role in the IBIEC process (Linnros and Hólmen, 1986). However, other studies, where no channeling effect was observed for surface amorphous layers (Williams et al., 1985b; Elliman et al., 1986), suggested that defects created away from the interface on the crystalline side played no role. Experiments with buried amorphous layers and measuring IBIEC rates under channeling conditions were more conclusive (Williams et al., 1985b; Elliman et al., 1986). A large reduction in IBIEC growth rate was observed for the near-surface interface of the buried layer (40–100%), compared with a random case. However, again such results were interpreted differently (Williams et al., 1985b; Priolo and Rimini, 1990; Elliman et al., 1986) to argue for either a role of mobile defects from the crystalline side or, alternatively, displacements produced exactly at the interface, as the main contribution to IBIEC. A more recent example of the channeling effect on IBIEC for a buried amorphous layer is shown in Figure 13 (Williams et al., 2000). Here, the regrowth differences are compared for channeled and random irradiations of an initially 1000 Å amorphous layer with 2 MeV C ions at 320°C to a dose of 1.2×10^{16} cm^{-2} in each case. Clearly, the front interface under channeling grows only 60% of that under random alignment, whereas the rear interface appears to show no differences between the two irradiations. The authors of this study (Williams et al., 2000) argued that, if mobile defects from the crystalline side were dominating IBIEC, then a much larger effect should have been expected. This conclusion is based on the difference in the magnitude of the nuclear energy deposition in the crystal between channeling and random alignments (whereby the channeled value is only about 5–10% of the random case). However, it was also argued that more detailed simulations would be necessary before a more precise determination of the origin of defects responsible for IBIEC could be made, as we illustrate in Section 4.

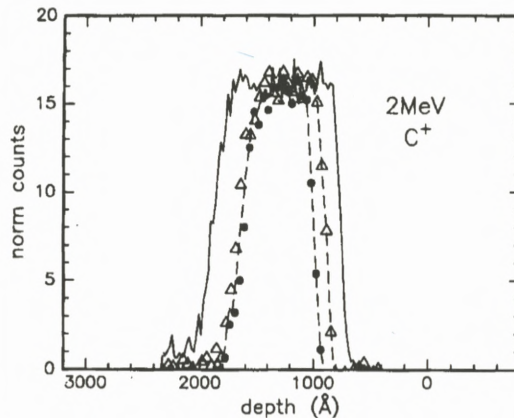

Figure 13. Random and channeled IBIEC regrowth extracted from RBS/channeling spectra (1.8 MeV He ions) for a 1000 Å amorphous silicon layer buried about 1000 Å below the surface. The data has been corrected for channeled He energy loss effects. The 2 MeV C ion dose was 1.2×10^{16} cm^{-2} in both random (filled circles) and channeled (open circles) cases. After Williams et al. (2000).

3.4. IBIEC Models

Priolo and Rimini (1990) have given an overview of various models to explain IBIEC observations up to about 1990. An early proposal suggested that annealing processes, which occur in the quenching of thermal spikes that overlap the amorphous-crystalline interface, were responsible for IBIEC (Kachurin, 1980). In addition, minimum free energy arguments and differences in free energy of amorphous and crystalline silicon have also been used to explain the temperature dependence of ion-induced amorphisation and crystallisation (Atwater et al., 1988). However, such proposals do not address many of the observations and fail to suggest the "defects" that may stimulate IBIEC. Furthermore, vacancies were suggested by several authors (Linnros et al., 1988a; Lulli et al., 1988; Nakata et al., 1981) as the prime defect involved. Firstly, the similarity of the initial activation energy of IBIEC (around 0.3 eV) to that of vacancy migration led Linnros et al. (1988a) to propose that migrating vacancies, produced athermally by the ion beam, mediated IBIEC, whereas, if the temperature was lowered, then the increased stability of divacancies, with a dissociation energy of 1.2 eV, may cause amorphisation at the interface. This two-defect model qualitatively explains both the layer-by-layer amorphisation and IBIEC processes but presupposes the migration of such defects in crystalline silicon to the interface. Other defects proposed to mediate IBIEC are (charged) kinks (Williams et al., 1985b; Priolo and Rimini,

1990) and dangling bonds (Mosley and Paesler, 1984) that are formed athermally by the ion beam directly at the interface. A difficulty with a single defect model is the fact that the apparent activation energy of IBIEC has been shown to vary from about 0.18 to 0.4 eV (see Figure 12b), which led Kinomura et al. (1999) to suggest that the rate limiting effect in IBIEC may involve several different defect-mediated processes, depending on the cascade density at the interface and the temperature. This proposal does not necessarily preclude kinks or other specific interface defects as the final step in the IBIEC process, but rather suggests that more complex defect processes may be involved in the annealing of dense cascades before discrete kinks are formed. A particular concern of vacancy models is that there is now considerable weight to arguments suggesting that defects produced right at the interface dominate IBIEC, as we illustrate more clearly in Section 4.

Another explanation for both layer-by-layer amorphisation and IBIEC is due to Jackson (1988), who developed an intracascade model in which each ion penetrating through the interface creates a disordered zone. Subsequent local interaction between defects in this zone can either lead to amorphisation or crystallisation. The onset of either amorphisation or crystallisation is controlled by a rate equation in which the net rate of interface movement, R, is given by the difference between a crystallisation term, Rx, and an amorphisation term, Rà, according to:

$$R = \frac{dx}{d\varphi} = R_x - R_\alpha, \tag{2}$$

where x is the distance of interface motion and φ is the ion beam dose. The amorphisation term can be written as $R_\alpha = V_\alpha \varphi$, where V_α is the volume of the amorphous zone created by a single ion. Crystallisation arises when defects produced by the ion beam annihilate in pairs at the interface. The simplicity of the Jackson model is attractive but it does not adequately account for ion mass and flux effects. Indeed, no single model appears to adequately explain all observations. We now move on to more recent channeling measurements and simulations that address more directly the origin of defects that influence IBIEC.

4. Cascade Effects on IBIEC: Observations and Interpretation

4.1. Experimental Observations

In this section, we present more detailed results of IBIEC rates obtained with random and channeled incident beams (Azevedo et al., 2002). In this study the recrystallisation rates of both surface and buried amorphous layers were studied with high resolution by *in situ* time resolved reflectivity (TRR) and *ex situ* RBS analysis.

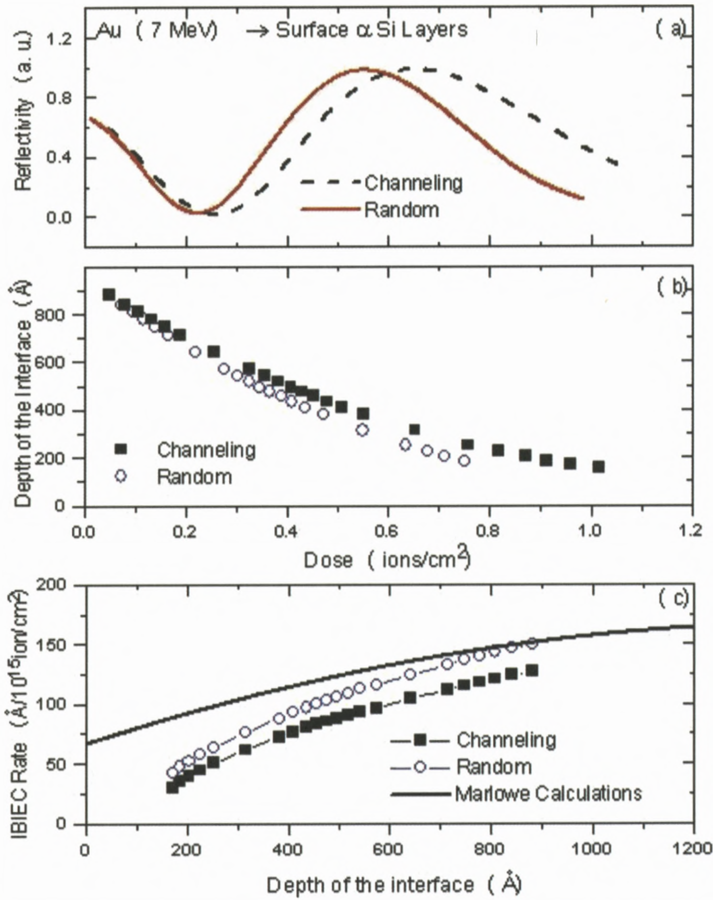

Figure 14. (a) Experimental reflectivity traces, as a function of dose, for 7 MeV Au ions irradiating a surface amorphous layer in silicon. The solid and dashed lines correspond to the random and channeling irradiations, respectively. (b) Depth of the interface as a function of the ion dose. (c) IBIEC rates for channeling (solid symbols) and random (open symbols) cases as a function of the interface depth. The solid line corresponds to MARLOWE calculations for the number of vacancies produced per ion per Å at the interface. After Azevedo et al. (2002).

In Figure 14, we present the results for surface amorphous layers in silicon irradiated under both random and channeling conditions (Azevedo et al., 2002). The experimental TRR traces for random (dashed line) and channeling (solid line) cases are plotted in panel (a). Note that for TRR from silicon using a 6328 Å laser, every 330 Å traversed by the interface corresponds to an oscillation between a maximum and a minimum of the reflectivity. Our results clearly indicate a reduc-

tion of the recrystallisation rate under channeling bombardment. This difference can be better appreciated by an examination of panels (b) and (c), where we plot, respectively, the interface depth as a function of the irradiation dose and the IBIEC rate as a function of the interface depth. These curves indicate that the magnitude of the channeling effect on interface motion is quite small in this case. For example, the maximum difference in the interface depths is of the order of 80 Å, whereas the IBIEC rate for channeling implants is only 20% smaller than the rate observed for random implants.

Unlike the results presented above, in previous measurements of IBIEC induced by 1.5 MeV Ne^+ (Williams et al., 1985a, 1985b) and 2.0 MeV C^+ (Williams et al., 2000) (see Figure 13) in samples consisting of an amorphous silicon surface layer, no channeling effect was observed. The lack of channeling effect was interpreted by Williams et al. (1985a) as evidence that displacements produced exactly at the interface were responsible for IBIEC. However, in these experiments the interface movement was monitored by RBS/channeling with alpha particles with energies between 1.5 and 1.8 MeV. Hence, limited depth resolution (even in the glancing angle backscattering geometry) of RBS (see Figure 13), means that RBS will not detect 20% reduced IBIEC growth under channeling conditions when this difference is of the order of the depth resolution.

In Figure 15, we present results of IBIEC for buried amorphous layers in silicon (Azevedo et al., 2002). In this case, the simultaneous movement of two amorphous-crystalline interfaces produces complicated patterns on the TRR traces, making their interpretation less evident than in the case of surface amorphous layers. For the sake of clarity, we only present IBIEC results extracted from RBS analysis of samples irradiated with increasingly higher doses. Panel (a) displays the RBS spectra for the buried layer before irradiation (solid line) and after 3×10^{15} Au/cm^2 random and channeling bombardments (squares and circles, respectively). Again, a clear channeling effect is observed. This difference is better quantified by an inspection of panel (b), where we plot the position of the amorphous-crystal interfaces as a function of the ion dose. It is apparent in this figure that the deeper interface (circles) advances at the same rate (281 ± 10 Å and 274 ± 14 Å per 10^{15} ions cm^{-2}) for channeling and random implants, respectively. However, the shallower interface (squares) advances much faster in random irradiations than in channeling cases (262 ± 10 Å and 124 ± 5 Å per 10^{15} ions cm^{-2}, respectively). A similar channeling effect was reported by Linnros and Hólmen (1986) for IBIEC in buried layers induced by 300 keV N and Ne beams and by Williams et al. (2000) in experiments with a 2 MeV C beam.

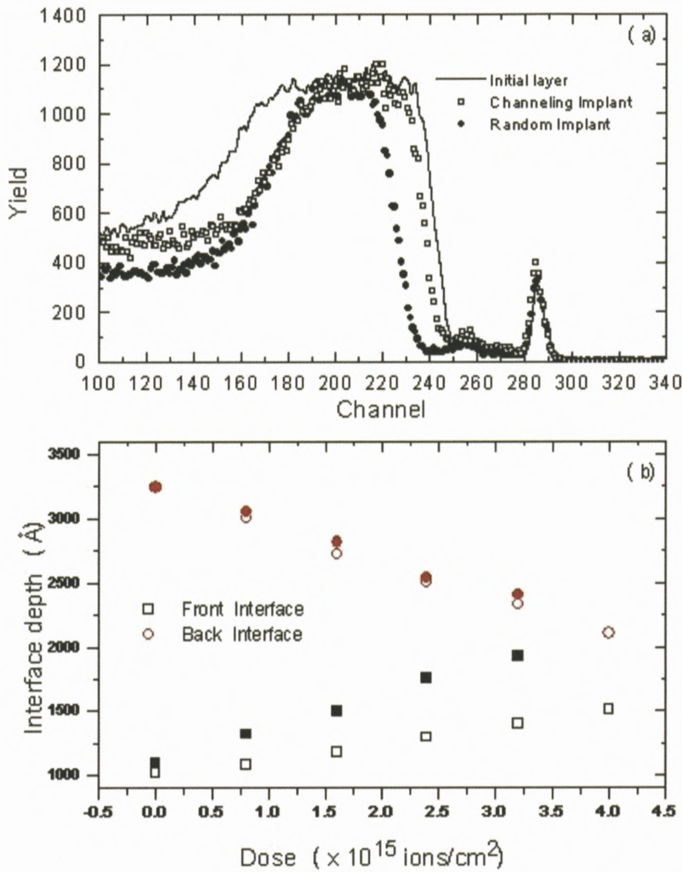

Figure 15. (a) RBS spectra for a buried amorphous layer irradiated with 1.6×10^{15} Au cm^{-2}. The solid line is the spectrum for the buried layer before the irradiation. Symbols (squares and circles) correspond to the random and channeling irradiations, respectively. (b) Position of the interfaces as a function of dose. Open and solid symbols correspond to channeling and random irradiations, respectively. After Azevedo et al. (2002).

4.2. Comparison with Simulations

The IBIEC growth data presented above are now compared with the results of computer simulations of collision cascades (atomic displacements). For the simulations, all displacements (point defects), both in random and channeled alignments, were calculated with the aid of the MARLOWE code (Robinson and Torrens, 1974; Robinson, 1990). MARLOWE has been specifically developed for the simulation of atomic displacements in both amorphous and crystalline

solids. The code is based on the binary collision approximation (BCA) (Azevedo et al., 1999) to construct particle trajectories. The atomic scattering is governed by screened potentials, such as ZBL (Ziegler et al., 1985) and Molière (1947). Thermal vibrations are simulated by a random gaussian distribution of the lattice atoms around their equilibrium positions, with amplitude given by the Debye–Waller (Eckstein, 1991) model. In the simulations performed here, we have used version 13c of the MARLOWE (Robinson, 1990) code with a ZBL potential to describe the Au-Si and Si-Si interactions and 490 K for the value of the silicon Debye temperature, in accordance with the results of references (Azevedo et al., 1999; Dygo et al., 1992; Hobler et al., 1996).

Figure 16a displays the result of MARLOWE calculations for a 300 Å surface layer (Azevedo et al., 2002). A reduction in the number of vacancies produced per ion per Å (η) in the crystalline region is apparent, even for random bombardments. This feature can be explained as follows. Even though the nuclear energy dissipation occurs mainly in cascades initiated by high energy primary knock ons, the average energy transferred to a silicon target atom by 7 MeV Au ions is of the order of 0.5 keV only. Such low energy primary knock-ons have a large critical angle for channelling (of the order of several degrees) and hence the number of displacement collisions that they initiate in crystalline silicon is less than in amorphous silicon. This explains the reduction of η in the crystalline region, even for a random orientation of the beam. Additional simulations show that the value of η in the crystalline region (Figure 16a) corresponds to the value predicted by MARLOWE for a random irradiation in a crystalline target without a surface amorphous layer. Furthermore, when the Au beam is aligned with the $\langle 100 \rangle$ channeling direction in the underlying crystalline silicon, the number of vacancies generated at the interface and within the crystalline region is lower than for the random case. Its also interesting to note that, under channeling conditions, η is slightly reduced in the amorphous region, in comparison with random implants. Simulations show that this difference is reduced as the thickness of the amorphous layer is increased. This latter observation implies that cascades initiated in the crystalline region can produce displacements in the amorphous region, even though it is closer to the surface. A comparison of the experimentally observed $\sim$20% lower IBIEC rate for channeling beam alignment with the simulation data in Figure 16a, indicates that the scale of difference between channeled and random IBIEC rates is most consistent with vacancies produced precisely at the interface than with vacancies produced in the amorphous or crystalline regions.

Figure 16b displays the results of simulations for a buried layer in silicon with the same configuration as those we have used in our experiments. It is apparent that, for channeling implants, η is strongly reduced in the crystalline region near to

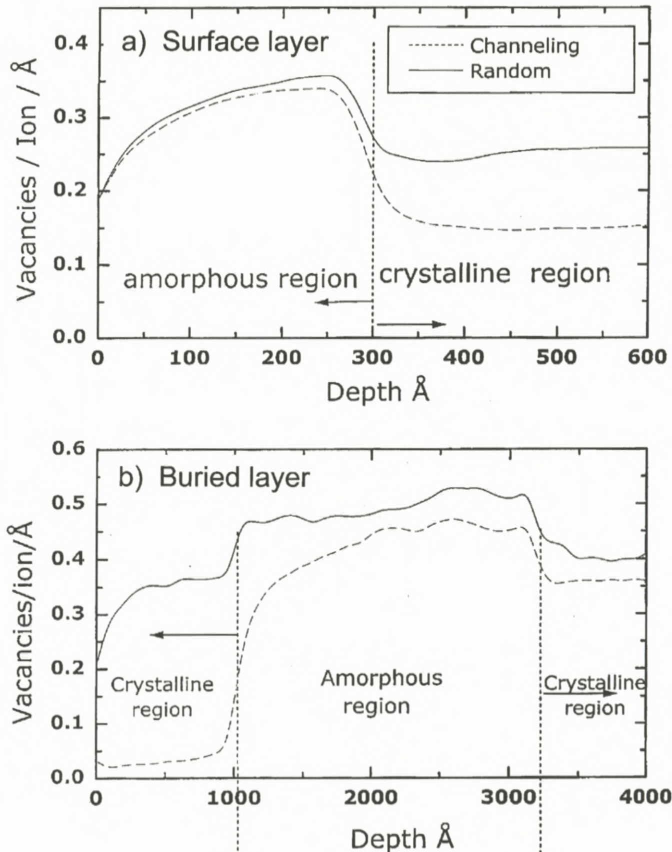

Figure 16. Point defect profiles calculated with MARLOWE for channeling (dashed lines) and random irradiations (solid lines) in surface and buried amorphous layers shown in upper and lower panels, respectively. After Azevedo et al. (2002).

the surface, as one might expect. However, only a small reduction of η is observed after the deeper interface. These features can be explained by the same arguments utilised above to explain the results for surface layers. Therefore, the most important feature displayed in Figure 16b is that, assuming IBIEC is controlled by point defects generated at the amorphous-crystalline interface, MARLOWE predicts a large channeling effect at the front interface and a very small effect at the back interface, consistent with our experimental data for a buried amorphous layer. Furthermore, the scale of the experimental IBIEC reduction under channeling conditions ($\sim$50%) appears to best correlate with the relative num-

ber of vacancies produced at the front interface (Figure 16b), rather than in the amorphous-crystalline regions, as we discuss below.

The solid line in Figure 14c corresponds to the predictions of MARLOWE for η at the amorphous-crystalline interface. As can be readily observed, η drops quickly as the interface approaches the surface. This feature is a result of the reduction in the cascade density for shallow depths and the experimental IBIEC rates (γ) display a similar trend. However, γ is clearly steeper than η when the thickness of the amorphous layer is smaller than about 500 Å. The same dependence of γ with the thickness of the amorphous layer has been observed in previous experiments with 5 MeV Au (Kinomura et al., 2001) and 7 MeV I (Heera et al., 1995) ions, and this effect was attributed to diffusion of point defects in the amorphous layer. However, this proposal is not consistent with our channeling data, particularly the large front interface effect. We suggest that other effects could be responsible for this behaviour and for the discrepancies with MARLOWE predictions. For example, it has been demonstrated previously that the IBIEC rate is affected by defect interactions within individual cascades (i.e. the cascade density) as well as by defect interactions between cascades (Kinomura et al., 1999). This suggests that the observed thickness dependence of γ could be related to a distortion of the point defect profiles at the interface when the interface is close to the surface, due to cascade density differences and cascade interactions, rather than being related to point defect diffusion. Furthermore, Kinomura et al. (2001) have demonstrated that oxygen impurity atoms recoiling from the surface native oxide contribute partially to a decrease in the IBIEC rates close to the surface. Therefore, the comparison of MARLOWE predictions with the experimental results for shallow surface amorphous layers is not straightforward.

In order to more precisely determine the origin of the defects that control IBIEC, we will compare the ratio between the channeling and random IBIEC rates ($\Gamma = \gamma_c/\gamma_r$) to the ratio between the corresponding simulated defect profiles. Proceeding in this way, in particular for shallow surface layers, the chemical contamination and cascade interaction effects are cancelled out. As indicated earlier, an examination of our simulation results indicate that the observed channeling effect can be better quantitatively explained by assuming that defects produced at the interface control the IBIEC process. From our results for amorphous layers, we can exclude defects coming from the amorphous region since the simulations show that η is reduced by only ~5% (surface layer) or 10% (buried layer) in that region while the observed channeling effect is of the order of 20% and 50% for surface and buried layers, respectively. On the other hand, the simulations for a buried layer indicate that defects produced in the crystalline region are not likely to be participating in IBIEC, since the simulations predict a 90% reduction of

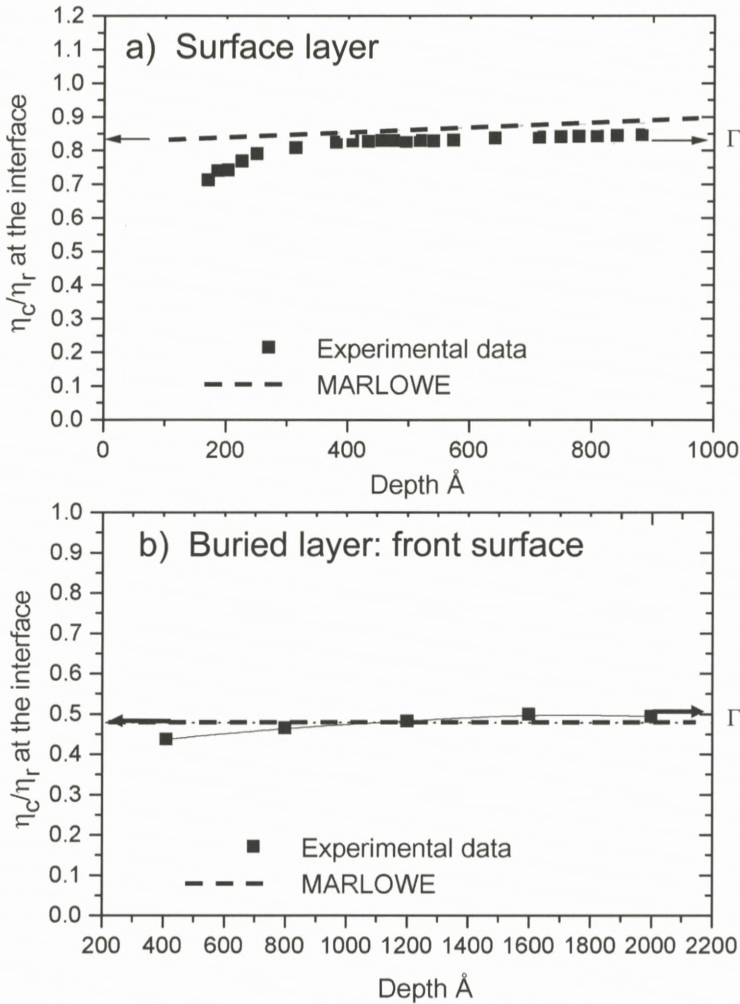

Figure 17. Ratio of η_c/η_r between the experimental growth rates and the calculated displacements at the interfaces. Upper and lower panels depict results for surface and buried layers, respectively. Adapted from Azevedo et al. (2002).

η in the crystalline region close to the surface, while the observed channeling effect is of the order of 50%. In Figure 17, adapted from the data of Azevedo et al. (2002), we present the ratio Γ between the experimentally determined IBIEC rates under channeling and random conditions, compared to the ratio between the corresponding calculated defect levels (η_c/η_r) at the amorphous-crystalline

interface. As can be observed, the magnitude of the experimentally determined Γ is in good agreement with MARLOWE calculations for the ratio η_c/η_r. Therefore, combining all experimental and simulation comparisons, we conclude that defects produced at or very near the amorphous-crystalline interfaces are most likely to control IBIEC. Although the precise interface defect controlling IBIEC is not revealed by these results, the data is consistent with any crystallisation-enabling defect, such as a kink, produced at the interface by the ion beam.

5. Some Answered and Unanswered Questions

In terms of disorder, defect generation and amorphisation in silicon, a reasonable qualitative description of observed phenomena exists. For example, for a given ion at fixed fluence and flux (or temperature and flux), it is possible to model the observed build up of disorder with temperature (fluence). It is also possible to model the accumulation of interstitial-based defects, located mostly near the ion's end-of-range, that evolve into line defects and loops on annealing. In contrast, a vacancy excess exists towards surface, evolving into voids on annealing. It is also known that mobile defects are gettered to and trapped at pre-existing defects and at the surface both during irradiation at elevated temperature (leading to the local nucleation of amorphous layers) and during subsequent annealing (leading to defect accumulation away from the depth of the maximum in nuclear stopping power).

The key deficiency in our understanding of ion-induced disorder and amorphisation relates to the lack of availability of quantitative models (with predictability) to treat defect accumulation and evolution. Available quantitative models (e.g. kinetic Monte Carlo and MD simulations) are only partially successful at best at describing observations when dynamic annealing is important during irradiation. Similarly, models of defect evolution on annealing are also not quantitative in most cases, since they rely on a precise knowledge of little-known defect parameters such as concentration and activation energies for defect formation, migration and annihilation. Defect gettering to and trapping at other defects can often control disorder accumulation and amorphisation behaviour but few data and models exist to describe such processes. Finally, a major unknown involves how cascade energy density determines defect generation and residual disorder. For example, amorphisation is not scalable with ion mass and flux and appears to depend in a complex manner on cascade density as well as instantaneous and average defect generation rates.

In terms of ion beam induced epitaxial crystallisation, there are several features of the phenomenon that are known and work well. For example, there is

now strong evidence that the process is driven by atomic displacements at the amorphous-crystalline interface. The Marlowe simulation code that calculates atomic displacements for random and channeled ion irradiations can successfully predict the effect of channeling on IBIEC growth (ie linear scaling of growth rate with atomic displacements at the interface) for individual ion species. The excellent agreement of simulations with experiment, suggests that individual values used in the simulations are accurate, such as nuclear energy deposition, atomic displacement distributions for random and aligned irradiations, as well as multiple scattering through amorphous layers and associated angular spreads.

The issue that is not understood at all well is the effect of cascade density on IBIEC. For example, the dependence of IBIEC on ion mass has no understandable scaling and the trends are the exact opposite to those for the ion mass dependence observed for amorphisation. Finally, if the driving force for IBIEC is atomic displacements at the amorphous-crystalline interface then the interface "defects" that mediate IBIEC are not known.

References

Atwater H.A., Thompson C.V. and Smith H.I. (1988): Interface-limited grain-boundary motion during ion-bombardment. Phys Rev Lett **60**, 112–115

Azevedo G. de M., Martini J.C., Behar M. and Grande P.L. (1999): Depth profiles and amorphization behavior under channeling condutions for low energy Bi ions implanted into Si crystals. Nucl Instrum Meth B **149**, 301–311

Azevedo G. de M., Williams J.S., Young I.M., Conway M.J. and Kinomura A. (2002): In-situ measurements of the channeling dependence of ion-beam-induced recrystallization in silicon. Nucl Instrum Meth B **190**, 772–776

Cannavo S., La Ferla A., Rimini E., Ferla G. and Gandolfi L. (1986): Ion-beam annealing during high-current density implants of phosphorous into silicon. J Appl Phys **59**, 4038–4042

Christel L.A., Gibbons J.F. and Sigmon T.W. (1981): Displacement criterion for amorphization of silicon during ion-implantation. J Appl Phys **52**, 7143–7146

Dennis J.R. and Hale E.B. (1978): Crystalline to amorphous transformation in ion-implanted silicon – Composite model. J Appl Phys **49**, 1119–1127

Dygo A., Smoulders P.J.M. and Boerma D.O. (1992): Simulation analysis of ion channeling spectra – Thermal vibrational amplitude in Si. Nucl Instrum Meth B **64**, 701–705

Eckstein W. (1991) Computer Simulation of Ion-Solid Interaction. Springer, Berlin

Elliman R.G., Williams J.S., Maher D.M. and Brown W.L. (1986): Kinetics, microstructure and mechanisms of ion beam induced epitaxial crystallisation of semiconductors. Mat Res Soc Symp Proc **51**, 319

Elliman R.G., Williams J.S., Brown W.L., Leiberich A., Maher D.A. and Knoell R.V. (1987): Ion-beam-induced crystallization and amorphization of silicon. Nucl Instrum Meth Phys Res B **19–20**, 435–442

Elliman R.G., Linnros J. and Brown W.L. (1988): Amorphization of silicon by ion irradiation: The role of the divacancy. Mat Res Soc Symp Proc **100**, 363

Goldberg R.D. (1995): Ion-induced disordering processes in Silicon. PhD Thesis, University of Melbourne

Goldberg R.D., Elliman R.G. and Williams J.S. (1993): The kinetics of self ion amorphization of silicon. Nucl Instrum Meth Phys Res B **80–81**, 596–599

Goldberg R.D., Williams J.S. and Elliman R.G. (1995): Amorphization of silicon by elevated temperature ion irradiation. Nucl Instrum Meth Phys Res B **106**, 242–247

Goldberg R.D., Williams J.S. and Elliman R.G. (1999): Preferential amorphization at extended defects of self-ion-irradiated silicon. Phys Rev Lett **82**, 771–774

Heera V., Henkel T., Kögler R. and Skorupa W. (1995): Evidence for diffusion-limited kinetics of ion-beam-induced epitaxial crystallization in silicon. Phys Rev B **52**, 15776–15784

Heera V., Kögler R., Skorupa W. and Grötzschel R. (1993): Dose-rate dependence of the ion-beam-induced epitaxial crystallization in silicon. Nucl Instrum Meth Phys Res B **80–81**, 538–542

Hobler G., Simionescu A., Palmetshofer L., Jahnel F., Von Criegern R., Tian C. and Stingeder G. (1996): Verification of models for the simulation of boron implantation into crystalline silicon. J Vac Sci Technol B **14**, 272–277

Howe L.M. and Rainville M.H. (1987): Heavy-ion damage in silicon and germanium. Nucl Instrum Meth Phys Res B **19–20**, 61–66

Jackson K.A. (1988): A defect model for ion-induced crystallization and amorphization. J Mater Res **3**, 1218–1226

Kachurin G.A. (1980): Mechanism of ion-stimulated crystallization of amorphous layers. Sov Phys Semicond **14**, 461–462

Kennedy E.F., Csepregi L., Mayer J.W. and Sigmon T.W. (1977): Influence of 0-16, C-12, N-14 and Noble-gases on crystallization of amorphous Si layers. J Appl Phys **48**, 4241–4246

Kinomura A., Williams J.S. and Fuji K. (1999): Mass effects on regrowth rates and activation energies of solid phase epitaxy induced by ion beams in Silicon. Phys Rev B **59**, 15214–15224

Kinomura A., Chayahara A., Tsubouchi N., Heck C., Horino Y. and Miyagawa Y. (2001): Movement of defects and atoms during ion beam induced crystallization. Nucl Instrum Meth B **175–177**, 319–323

Linnros J and Hólmen G. (1986): Channeling dependence of ion-beam-induced epitaxial recrystallization in silicon. J Appl Phys **59**, 1513–1517

Linnros J., Hólmen G. and Svensson B. (1985): Proportionality between ion-beam-induced epitaxial regrowth in silicon and nuclear-energy deposition. Phys Rev B **32**, 2770–2777

Linnros J., Brown W.L. and Elliman R.G. (1988a): Pulsed ion beam induced crystallization and amorphization of silicon. Mat Res Soc Symp Proc **100**, 369

Linnros J., Elliman R.G. and Brown W.L. (1988b): Divacancy control of the balance between ion-beam-induced epitaxial crystallization and amorphization in silicon. J Mater Res **3**, 1208–1211

Lulli G., Merli P.G. and Vittori Antisari M. (1987): Solid-phase epitaxy of amorphous-silicon induced by electron irradiation at room-temperature. Phys Rev B **36**, 8038–8042

Lulli G., Merli P.G. and Vittori Antisari M. (1988): Solid phase epitaxy of implanted silicon by electron irradiation at room temperature. Mat Res Soc Symp Proc **100**, 375

Maher D.M., Elliman R.G., Linnros J., Williams J.S., Knoell R.V. and Brown W.L. (1987): Epitaxial crystallization of amorphous silicon layers under ion irradiation: Orientation dependence. Mat Res Soc Symp Proc **93**, 87

Molière G. (1947): Theorie der Streuung schneller geladener Teilchen, 1. Z Naturforsch Sect A-A J Phys Sci **2**, 133–145

Morehead F.F. Jr., Crowder B.L. and Title R.S. (1970): Formation of amorphous Si by ion bombardment as a function of ion, temperature and dose. Bull Amer Phys Soc **15**, 396

Mosley L.E. and Paesler M.A. (1984): Electronic effect on crystallization growth velocities produced by charged dangling bonds in A-Si. Appl Phys Lett **45**, 86–88

Nakata J., Takahashi M. and Kajiyama K. (1981): Insitu self ion-beam annealing of damage in Si during high-energy (0.53 MEV–2.56 MEV As^{+} ion-implantation. Jpn J Appl Phys **20**, 2211–2221

Olson G.L. and Roth R.A. (1988): Kinetics of solid phase crystallization in amorphous silicon. Mat Sci Rep **3**, 1

Poate J.M., Jacobson D.C., Williams J.S., Elliman R.G. and Boerma D.O. (1987): Diffusion of implanted impurities in amorphous Si. Nucl Instrum Meth B **19–20**, 480–483

Poate J.M., Linnros J., Priolo F., Jacobson D.C., Batstone J.L. and Thompson M.O. (1988): Nonequilibrium segregation and trapping phenomena during ion-induced crystallization of amorphous Si. Phys Rev Lett **60**, 1322–1325

Priolo F. and Rimini E. (1990): Ion-beam-induced epitaxial crystallization and amorphization in silicon. Mat Sci Rep **5**, 319

Priolo F., Spinella C., La Ferla A., Battaglia A., Rimini E., La Ferla G., Carnera A. and Gasparotto A. (1989a): Ion-assisted regrowth of deposited Si layers: Mechanism and morphology. Mat Res Soc Symp Proc **128**, 563

Priolo F., Spinella C., La Ferla A., Rimini E. and La Ferla G. (1989b): Ion-assisted recrystallization of amorphous silicon. Appl Surf Sci **43**, 178–186

Priolo F., Spinella C. and Rimini E. (1990): Phenomenological description of ion-beam-induced epitaxial crystallization of amorphous-silicon. Phys Rev B **41**, 5235–5242

Robinson M.T. (1990): The temporal development of collision cascades in the binary-collision approximation. Nucl Instrum Meth B **48**, 408–413

Robinson M.T. and Torrens I.M. (1974): Computer-simulation of atomic-displacement cascades in solids in binary-collision approximation. Phys Rev B **9**, 5008–5024

Spaepen F. and Turnbull D. (1982): Crystallization processes. In: Poate J.M. and Mayer J.W. (Eds), Laser Annealing of Semiconductors. Academic Press, New York, p 15

Swanson M.L. and Quennevi A.F. (1971): Effect of compressional plastic deformation on superconducting transition temperature of indium and tin. Scripta Metall **5**, 1081

Takeda S., Kohyama M. and Ibe (1994): Interstitial defects on (113) in Si and Ge – Line defect configuration incorporated with a self interstitial atom chain. K Phil Mag A **70**, 287–312

Vook F.L. and Stein H.J. (1969): Relation of neutron to ion damage annealing in Si and Ge. Rad Eff **2**, 23

Williams J.S. (1992): Subsurface processing of electronic materials assisted by atomic displacements. MRS Bull **17**, 47–51

Williams J.S. (1994): Ion induced damage and dynamic annealing processes. Trans Mat Res Soc Jpn **17**, 417

Williams J.S. (1998): Unpublished article

Williams J.S. and Elliman R.G. (1983): The role of electronic processes in epitaxial recrystallisation of amorphous semiconductors. Phys Rev Lett **51**, 1069–1072

Williams J.S., Elliman R.G., Brown W.L. and Seidel T.E. (1985a): Beam induced crystallisation of silicon. Mat Res Soc Symp Proc **37**, 127

Williams J.S., Elliman R.G., Brown W.L. and Seidel T.E. (1985b): The dominant influence of beam induced interface rearrangements on solid phase epitaxial crystallisation of amorphous silicon. Phys Rev Lett **55**, 1482–1485

Williams J.S., Goldberg R.D., Petravic M. and Rao Z. (1994a): Phase transformations and compound formation during ion irradiation of material. Nucl Instrum Meth Phys Res B **84**, 199–203

Williams J.S., Tan H.H., Goldberg R.D., Brown R.A. and Jagadish C. (1994b): Dynamic annealing & amorphous phase formation in Si, GaAs, AlGaAs under ion irradiation. Mat Res Soc Symp Proc **316**, 15

Williams J.S., Young I.M. and Conway M.J. (2000): Ion-beam-induced epitaxy experiments in silicon under channeling and random alignments. Nucl Instrum Meth Phys Res B **161–163**, 505–509

Ziegler J.F., Biersack J.P. and Littmark U. (1985): The Stopping and Range of Ions in Solids. Pergamon, New York